

## Aberystwyth University

### *A tale of two rift shoulders and two ice masses:*

Le Heron, Daniel P.; Busfield, Marie; Ali, Dilshad; Vandyk, Thomas; Tofaif, Saeed

*Published in:*  
Geological Society Special Publications

*DOI:*  
[10.1144/SP475.11](https://doi.org/10.1144/SP475.11)

*Publication date:*  
2018

*Citation for published version (APA):*

Le Heron, D. P., Busfield, M., Ali, D., Vandyk, T., & Tofaif, S. (2018). A tale of two rift shoulders and two ice masses: the Cryogenian glaciated margin of Death Valley, California. *Geological Society Special Publications*, 475. <https://doi.org/10.1144/SP475.11>

#### **General rights**

Copyright and moral rights for the publications made accessible in the Aberystwyth Research Portal (the Institutional Repository) are retained by the authors and/or other copyright owners and it is a condition of accessing publications that users recognise and abide by the legal requirements associated with these rights.

- Users may download and print one copy of any publication from the Aberystwyth Research Portal for the purpose of private study or research.
- You may not further distribute the material or use it for any profit-making activity or commercial gain
- You may freely distribute the URL identifying the publication in the Aberystwyth Research Portal

#### **Take down policy**

If you believe that this document breaches copyright please contact us providing details, and we will remove access to the work immediately and investigate your claim.

tel: +44 1970 62 2400  
email: [is@aber.ac.uk](mailto:is@aber.ac.uk)

1 **A tale of two rift shoulders, and two ice masses: the Cryogenian glaciated**  
2 **margin of Death Valley, California.**

3  
4  
5 LE HERON, D.P.<sup>1</sup>., BUSFIELD, M.E.<sup>2</sup>., ALI, D.O.<sup>3</sup>., VANDYK, T.<sup>4</sup>., TOFAIF, S.<sup>5</sup>.

6 *<sup>1</sup>Department of Geodynamics and Sedimentology, University of Vienna, Althanstrasse 14,*

7 *A-1090 Vienna, Austria*

8 *<sup>2</sup>Geography and Earth Sciences, Aberystwyth University, Llandinam Building, Aberystwyth,*  
9 *Ceredigion, SY23 3DB*

10 *<sup>3</sup>Department of Earth Sciences, Royal Holloway University of London, Egham, Surrey, TW20 0EX*

11 *<sup>4</sup>Department of Geography, Royal Holloway University of London, Egham, Surrey, TW20 0EX*

12 *<sup>5</sup>Saudi Aramco P.O. Box 5000. Dhahran 31311, Saudi Arabia*

13 *\*Corresponding author's e-mail address: [daniel.le-heron@univie.ac.at](mailto:daniel.le-heron@univie.ac.at)*

14  
15 **Abstract:** The Death Valley area of California, USA, exposes an outstanding record of a Neoproterozoic  
16 (Cryogenian) glaciated margin: the Kingston Peak Formation. Despite the quality of exposure, however, the  
17 outcrops of glaciogenic strata are fragmentary, forming isolated, laterally offset outcrop belts at the western  
18 extremity of the Basin and Range province. Excellent evidence for glacially modulated sedimentation includes (i)  
19 ice-rafted dropstones in most ranges, (ii) thick diamictites bearing a variety of exotic (extrabasinal) clasts, (iii)  
20 striated clasts, and (iv) local occurrences of glaciectonic deformation structures at the basin margins. In tandem  
21 with this, there is a distinct signature of slope collapse processes in many ranges, including (i) up to km-scale  
22 olistoliths, (ii) extensional growth fault arrays, (iii) dramatic proximal-distal thickness changes and (iv) basalt  
23 occurrences. New sedimentological observations reinforce long-held views of rifting superimposed on glaciation  
24 (or vice versa), with both processes contributing to a complex record whereby rift and glacial processes vie for  
25 stratigraphic supremacy. We consider that a mechanism of diamictite accumulation in a series of rift-shoulder  
26 minibasins produced greatly contrasting successions across the Death Valley area, under the incontrovertible  
27 influence of hinterland ice sheets.

28

29

30

31

32

33 The Death Valley area yields world class exposures of Cryogenian strata (Prave, 1999),  
34 which record the influence of glaciogenic and rift-related fluxes of sediment into a  
35 subaqueous basin (Prave, 1999; Macdonald et al., 2013; Busfield & Le Heron, 2016; Le  
36 Heron & Busfield, 2016; Le Heron et al., 2017). During the Cryogenian, two glaciations of  
37 potentially global extent have been proposed, the older Sturtian and younger Marinoan  
38 (Hoffman & Schrag, 2002), with the record of both glaciations argued to be contained within  
39 the lower and upper parts of the Kingston Peak Formation (KPF) in this region (Macdonald et  
40 al. 2013). Worldwide, these glaciations have been attributed to cooling under a long-lived and  
41 globally synchronous Snowball Earth (see Hoffman et al. 2017 for review). However,  
42 arguments against global glaciation have favoured deposition of Cryogenian diamictite-  
43 dominated successions as rift-related mass flows subject to a substantially reduced, Alpine-  
44 style glacial influence (Eyles & Januszczak, 2004). The Death Valley region offers ideal  
45 sections to illustrate the combined influence of glaciogenic sediment flux from marine-  
46 terminating ice masses and syn-sedimentary rift activity, where the influence and relative  
47 dominance of both sources of sediment can be distinguished. The structural and  
48 sedimentological record of the active tectonic regime is variable across the study region, and  
49 hence a basin-wide review of the studied sections is provided herein. This review sheds  
50 significant light on the palaeogeographic setting of Cryogenian glaciation in this region,  
51 offers a blueprint for recognising rift-related sedimentation on a glaciated margin otherwise  
52 dominated by glaciogenic sediment flux, and raises questions about the validity of regional  
53 chronostratigraphic units where the possibility of diachronous rifting and glaciation remains  
54 to be addressed.

55 The Death Valley region lies toward the west of the Basin and Range province where  
56 Cenozoic tectonism, with a significant strike-slip component and localised hyper-extension,  
57 has disassembled a once more continuous belt of Neoproterozoic strata (**Fig. 1A**). A range of  
58 estimates are available concerning the magnitude of extension which has affected the region  
59 since the Mesozoic. Taking into account both Mesozoic compression and Cenozoic  
60 extension, Levy and Christie-Blick (1989) estimated an extension factor of about 150%.  
61 Dextral strike-slip faults have also offset some of the outcrops, with the Amargosa canyon a  
62 notable example (Guest et al., 2003). At a regional scale, palinspastic reconstructions of the  
63 eastern part of the area (encompassing the Silurian Hills, Alexander Hills, Kingston Range  
64 and Sperry Wash outcrop belts, **Fig. 1 A**) show comparatively minor dislocation, with much  
65 of the E-W strike-slip motion accommodated by a kink in the Garlock Fault at Owlshead

66 Mountains (Fridrick and Thompson, 2011). This relatively minor offset of the eastern outcrop  
67 belts, alongside their exceptionally high-quality exposure, affords far greater correlation of  
68 individual sedimentary sequences, and thus significantly enhances the scope for generating  
69 meaningful palaeogeographic reconstructions.

70 The disparate and disconnected arrangement of Neoproterozoic outcrop belts throughout the  
71 Death Valley region has focussed efforts on first order correlation of the KPF (e.g. the  
72 stratigraphic framework of Prave, 1999). Macdonald *et al.* (2013) developed the stratigraphic  
73 framework of Prave (1999) and proposed a five-fold tectonostratigraphic subdivision of the  
74 KPF (TU0-4, Macdonald *et al.*, 2013). Of these, four (TU0 and TU2, 3, 4) were argued to be  
75 present in Death Valley. The original stratigraphy of Prave (1999) broadly recognises a basal,  
76 non-glacial marine succession (KP1: genetically unrelated to the remainder of the  
77 succession), KP2 (a basal diamictite), and KP3 (mass flow deposits, olistostromes).  
78 Macdonald *et al.* (2013) considered that KP2 and KP3 were the equivalent of the Sturtian  
79 glaciation in Australia, with KP4 its Marinoan counterpart. A well-developed interglacial  
80 stratigraphy is not universally present across the Death Valley outcrop belts, but is well  
81 expressed in the Panamint Range where various limestones separate KP3 from KP4  
82 diamictites (Miller, 1985; Prave, 1999; Petterson *et al.*, 2011). The uppermost diamictites  
83 have been argued to represent younger, Marinoan-age deposits (Prave, 1999; Macdonald *et*  
84 *al.*, 2013).

85 Whilst the attempts at stratigraphic subdivision outlined above are valuable, there are certain  
86 limitations. Even at comparable stratigraphic levels, lateral lithofacies variations are very  
87 pronounced, leading to practical difficulty in applying the five-fold framework routinely  
88 across studied sections. The most noteworthy example in this region is the evidence for the  
89 younger 'Marinoan' equivalent diamictite (widely referred to as unit KP4; Macdonald *et al.*  
90 2013). Though recognised as only a locally-developed unit, its presence has been reported  
91 throughout the wider Death Valley region, from the westernmost Panamint Range (Miller,  
92 1985; Prave, 1999; Petterson *et al.*, 2011), through the central Saddle Peak Hills within the  
93 National Park itself (Creveling *et al.*, 2016), to the Kingston Range and neighbouring  
94 outcrops further east (Mrofka & Kennedy, 2011; Macdonald *et al.*, 2013). Yet detailed  
95 sedimentological investigation of the latter sections reveals no evidence for a significant  
96 break in the stratigraphic succession which would distinguish a younger 'KP4' unit from the  
97 predominant 'Sturtian' equivalent strata (units KP2 and KP3). The diamictite facies  
98 association present towards the top of the exposed sequence is closely interbedded with



99 graded sandstones and sandy, matrix-rich conglomerates, genetically continuous with the  
100 preceding KP2-3 coarse-clastic strata (Le Heron et al., 2014, 2017; Le Heron and Busfield,  
101 2016). Overall, the diamictite facies represent a proximal component of an overall  
102 coarsening-upward sequence. This is interpreted to record progradation of a subaqueous fan  
103 during a single protracted glaciation (Le Heron et al., 2017), albeit subject to multiple cycles  
104 of ice advance and recession, but lacking robust evidence for a second, considerably younger  
105 glaciation.

106

### 107 **Death Valley glacial geology at a glance**

108 Given the geographic separation of the various Death Valley outcrop belts for the reasons  
109 given above, we provide a synthesis of the stratigraphy and sedimentology of each of the  
110 main outcrop belts below. Troxel (1966, 1982) suggested that the KPF exhibited distinct  
111 northern and southern facies characteristics, with the two facies groupings recording different  
112 source areas. This idea was more fully developed in Wright et al. (1974) who proposed a  
113 northern source area (the Nopah uplands) and a southern source area (the Mojave uplands).  
114 There have been further attempts to subdivide the outcrop belts into east-west groupings  
115 (Mrofka, 2010). Collectively, the KPF records an excellent archive of (i) glacially-influenced  
116 sedimentation, and (ii) rift processes, but not all outcrop belts exhibit these characteristics to  
117 the same degree. Thus, a systematic evaluation of each outcrop belt is important in order that  
118 here the region can be understood as a whole, and a palaeogeographic synthesis can be  
119 attempted.

120

#### 121 *The Sperry Wash section*

122 Located immediately north of the Dumont Dunes along the northern flank of the Amargosa  
123 River (see **Fig. 1** for location), the Sperry Wash succession was first logged in 1963 by  
124 Bennie Troxel, although the logged section itself was published some time later (Troxel,  
125 1982), where excellent descriptions were provided. Rare striated and faceted clasts were  
126 reported in a succession that was estimated to be up to 40% Fe by volume (Troxel, 1982, p.  
127 62). Exactly 50 years later, in March 2013, careful logging of the complete 1 km thick  
128 succession to a vertical resolution of 50 cm revealed multiple examples of pebble to boulder-  
129 sized limestones that deflect, warp, or truncate underlying laminae in siltstone and shale

130 (Busfield and Le Heron, 2016). The complete section, included herein and modified from  
131 Busfield and Le Heron (2016) (**Fig. 2 A**), illustrates a well-defined coarsening-upward motif  
132 over several hundred metres in which interbedded conglomerates, sandstones and mudrocks  
133 occur. A thick diamictite interval appears near the top of the unit (**Fig. 2 A**). Collation of  
134 palaeocurrent data, including ripple foresets, scour marks, and flute casts, point to a  
135 predominant SE-directed palaeoflow during deposition with very little deviation from this  
136 trend (Busfield and Le Heron, 2016). Large parts of the succession are of outstanding outcrop  
137 quality and exhibit 100% exposure over many tens of metres (**Fig. 3 A**). Thick, tabular beds  
138 of sandstone or conglomerate (**Fig. 3 B**) commonly cap multi-metre scale coarsening up  
139 intervals; many of these show classic Bouma sequences (**Fig. 3 C**). At recurrent intervals,  
140 lonestones derived from the Beck Spring Dolomite occur in mudrocks, with clear evidence of  
141 lamina deflections beneath them (**Fig. 3 D**). Occasionally, dm-thick beds of muddy diamictite  
142 occur encased within shales (**Fig. 3 E**). In other instances, thick intervals of diamictite toward  
143 the top of the succession are interbedded with highly attenuated and strained sandstones (**Fig.**  
144 **3 F**). Other features include dewatering structures (**Fig. 3 G**). The recurrent fining-upward  
145 trends within individual beds extend to mudrocks, whereby grain size variations can be  
146 observed at the cm-scale (**Fig. 3 H**).

147 In spite of the outstanding exposure, and seemingly demonstrative sedimentary structures, the  
148 interpretation of the Sperry Wash section is not without controversy. Troxel and his students  
149 have traditionally interpreted the boulder-sized lonestones to result from slope foundering,  
150 causing large clasts to roll basinwards (Calzia *et al.*, 2000). By contrast, Busfield and Le  
151 Heron (2016) interpreted these lonestones as ice-rafted dropstones, an interpretation which is  
152 greatly strengthened by comparison to the Kingston Range sections (Le Heron and Busfield,  
153 2016). The interstratified conglomerates, sandstones and mudrocks are collectively  
154 interpreted as a spectrum of mass flows ranging from debrites to high and low density  
155 turbidites, sourced from a grounded marine ice mass (Busfield and Le Heron, 2016). The  
156 overall coarsening upward profile of the succession attests to a progressive ice advance, with  
157 the intensely folded and attenuated intervals near the top considered to represent  
158 glaciotectonites produced by sub-ice shearing at the grounding line (Busfield and Le Heron,  
159 2016). Considering this evidence, a picture emerges of an ice margin delivering mass flows to  
160 the basin. This general picture can be used to guide and develop the interpretations for several  
161 other Death Valley sections, as we shall demonstrate below.

162

163 *The Saddle Peak Hills section*

164 Mapping of the Saddle Peak Hills succession (Macdonald *et al.*, 2013) demonstrated that the  
165 KPF is cut through by a series of dip-slip faults, making an accurate measured section very  
166 difficult indeed. Nevertheless, the Saddle Peak Hills KPF succession comprises a lower c.  
167 300 m thick, intermittently exposed unit that bears great similarity to Sperry Wash, and an  
168 upper c. 50 m thick unit that contains large dolostone rafts interpreted to result from  
169 gravitational collapse of the Noonday Dolomite cap carbonate facies (Creveling *et al.*, 2016).  
170 The basal unit is very ferruginous, and we present a basic sedimentary log herein from the  
171 part of it (**Fig. 2 B**) which illustrates five key phenomena. These are (i) the occurrence of  
172 interbedded conglomerates, sandstones and mudrocks, (ii) the predominance of fining upward  
173 cycles at the bed scale, (iii) the development of bedset trends with both coarsening and fining  
174 upward motifs over many m of strata, (iv) well-expressed limestones deflecting underlying  
175 laminae and (v) sole marks including grooves and flute casts beneath sandstone beds. Our  
176 measured section is faulted into place, with the Beck Spring Dolomite lying directly below it  
177 (**Fig. 4 A**). Thick diamictite beds, >2 m in thickness, punctuate a succession otherwise  
178 dominated by normally-graded beds (**Fig. 4B**). The diamictites show a ferruginous matrix and  
179 a dominance of dolostone clasts sourced from the Beck Spring Dolomite (**Fig. 4 C**).  
180 Limestone-bearing horizons are sandwiched between normally-graded sandstone beds (**Fig. 4**  
181 **D**). The limestones are typically cm-sized (**Fig. 4 E, F**).

182         In the Saddle Peak Hills, the diamictites have identical relationships with sandstones  
183 and mudrocks as at Sperry Wash, where they are interpreted as debrites interrupting an  
184 otherwise turbidite-dominated succession, with a secondary glacial influence to produce  
185 dropstones (Busfield and Le Heron, 2016). This suite of features confirms the close similarity  
186 between the Saddle Peak Hills and Sperry Wash strata. By comparison to the Sperry Wash  
187 area, palaeocurrent data are few, but available measurements (**Fig. 2 B**) also support a SE-  
188 directed palaeoslope in this area. In both these areas, the stratigraphic position of the strata in  
189 a regional context is slightly ambiguous. In the Saddle Peak Hills, Macdonald *et al.* (2013)  
190 assigned them to a sub-unit of KP3.

191

192 *The Kingston Range outcrop belt*

193 The Kingston Range exposes the thickest exposures of the KPF. The deposits increase in  
194 thickness from about 500 m thick in the north (Le Heron et al., 2014) to about 2.5 km in the  
195 extreme south of the range (Le Heron et al., 2018). The succession was mapped at a regional  
196 scale by Calzia et al. (2000) who identified a large number of km-scale megaclasts of  
197 carbonate derived from the Crystal Spring Formation and the Beck Spring Dolomite  
198 “floating” within the succession. This general trend was borne out by detailed mapping in the  
199 central part of the range by Macdonald et al. (2013) who made similar observations. In terms  
200 of a general stratigraphic subdivision, Le Heron et al. (2018) proposed that the KPF was  
201 divisible into three main stratigraphic units in the southern part of the range, which are: (i) a  
202 basal diamictite, (ii) an olistostrome succession, and (iii) a supra-olistostrome succession  
203 (Fig. 2 C).

204 The lithofacies as described by Le Heron et al. (2018) can be summarised as follows.  
205 Continuous sections of turbidites characterise the basal part of the supra-olistostrome strata in  
206 the Kingston Range (Fig. 5 A). Sharp-based, normally graded conglomerates appear at  
207 intervals (Fig. 5 B), with abundant limestones in intercalated shales and sandstones (Fig. 5 C,  
208 D). Toward the top of the supra-olistostrome succession, diamictites appear (Fig. 5 E), the  
209 lower levels of which are intercalated with the graded sandstones. The diamictites include  
210 both massive (Fig. 5 E) and stratified varieties: the latter exhibit excellent dropstone textures  
211 (Fig. 5 F). Clasts have polished to furrowed surfaces (Fig. 5 G). On closer inspection, some  
212 of the polished clast surfaces are striated (Fig. 5 H).

213 Overall, the supra-olistostrome interval invites close comparison to Sperry Wash, both  
214 in terms of facies (graded sandstone beds punctuated by conglomerates) and stratigraphic  
215 motif (complex coarsening-up cycles). These reflect a gravity flow-dominated fan that was  
216 fed from a glacial source: the Kingston Range Fan (Le Heron et al., 2018). Given the context,  
217 and the exquisite deformation structures beneath many of the limestones, an ice-rafting  
218 mechanism seems most likely.

219 The regional palaeogeographic perspective of Le Heron and Busfield (2016) proposes  
220 a northern (Nopah) ice sheet that flowed to the SE (Fig. 1 B). Six lines of evidence underpin  
221 the interpretation of a SE-dipping palaeoslope in the Kingston Range. These are: (i) dramatic  
222 thickness variations from Beck Spring Canyon to the southernmost Kingston Range, from c.  
223 350 m to > 5 km; (ii) NW-SE striking faults that show clear evidence of stratal thickening on  
224 downthrown blocks to the SE (Walker *et al.*, 1986; Le Heron, 2015); (iii) sedimentological

225 evidence for flow evolution from debrites to low-density turbidites to the SE across the range,  
226 (iv) the existence of an olistostrome complex apparently derived from the NW-SE striking  
227 fault array that is not present to the NW; (v) dominant SE palaeocurrents recorded throughout  
228 the range, particularly in the low density turbidites exposed in the south of the range; (vi), at a  
229 local scale, evidence for bed thinning and stratal pinchout in a southeastward direction over  
230 several hundred metres. Thus, integrating these lines of evidence, we view the Kingston  
231 Range belt simply as a continuation of the Sperry Wash / Saddle Peak Hills slope. This slope  
232 drained the Nopah Highlands of Wright *et al.* (1974).

233

### 234 *The Silurian Hills outcrop belt*

235 The existence of diamictites equivalent to the KPF in the Silurian Hills was demonstrated  
236 during mapping campaigns almost 60 years ago (Kupfer, 1960). Since that time, until very  
237 recently the only detailed study in this outcrop belt was contained in the MS thesis of Basse  
238 (1978). A 1.4 km thick sedimentary log for this belt (**Fig. 2 D**) underscores the predominance  
239 of thick diamictite deposits together with lonestone-bearing, heterolithic deposits. Le Heron  
240 *et al.* (2017) recognised two distinct types of diamictite: (i) a boulder-bearing diamictite and  
241 (ii) a megaclast-bearing diamictite, which are repeatedly stacked throughout the 1.4 km thick  
242 succession (**Fig. 7A**). Clasts in the boulder-bearing diamictites predominantly comprise  
243 quartzite, felsic gneiss and schist, with some metabasite (schist grade) (**Fig. 7 B**). They are  
244 punctuated at intervals by heterolithic deposits characterised by repeated, bed-scale fining  
245 upward sequences (**Fig. 7 C**). Dropstones occur in multiple horizons (**Fig. 7 D**) and are  
246 typically composed of crystalline basement material (i.e. gneiss, schist, and granite).

247         Given that the clasts are of the same composition to the dropstones, the boulder-  
248 bearing diamictites were proposed to be derived from a glacial source. The megaclast  
249 diamictites, by contrast, were argued to be derived from slope failure and syn-sedimentary  
250 fault activity, essentially recording the collapse of a carbonate platform sequence that  
251 mantled the crystalline basement. The glacial “conveyor belt” supplied far travelled clasts  
252 both to boulder-bearing diamictites and as dropstones in heterolithic deposits, whilst  
253 megaclasts were largely supplied through foundering of the sedimentary succession that  
254 underlies the KPF. In sum, the sedimentological observations above are consistent with a  
255 subaqueous fan complex as first proposed by Basse (1978), with the newly recognised glacial  
256 influence (Le Heron *et al.*, 2017) superimposed. This, together with the occurrence of

257 lonestones throughout the more heterolithic parts of the succession (**Fig 7 D**) underscores a  
258 broadly common depositional environment to that identified further north in Sperry Wash.  
259 The key difference, as noted by Troxel (1966, 1982), is the *composition* of the lonestones and  
260 the predominance of basement lithologies in the boulder-bearing diamictite. The reason for  
261 this is the derivation of these from a southern source (the Mojave uplands: Wright et al.,  
262 1974).

263

#### 264 *The Southern Salt Spring Hills*

265 This region was last examined in the mid-1960s, when it was mapped by Troxel (1967). In  
266 2016, two of us (Le Heron and Vandyk) re-examined Troxel's units pCka-pCke: the mapping  
267 units which we interpret to belong to the KPF. We present a sketch log for part of this range  
268 (**Fig. 8**). All rocks have been contact metamorphosed to varying degrees as a result of the  
269 emplacement of a quartz diorite which underlies the range (Troxel, 1967). The base of the  
270 KPF is not exposed, and the succession commences with trough cross-bedded quartzites.  
271 Intervals of dolostone also occur low down in the succession. Unlike the other ranges, an  
272 accurate sedimentary log is virtually impossible owing to metamorphism and / or tectonic  
273 activity which have imparted a highly rubbly appearance to the outcrop (**Fig. 9 A**), meaning  
274 that even where well bedded strata are recognised, it is difficult to measure true thicknesses  
275 accurately. Massive, dark-coloured, ferruginous diamictites (**Fig. 9 B**) dominate the lower  
276 portion of the succession (**Fig. 9**), which are rich in gneiss, schist, quartzite and granite clasts  
277 varying from pebble to boulder size. The diamictite is punctuated by rare m-thick intervals of  
278 delicately laminated strata which contain abundant lonestones (**Fig. 9 C**). The middle part of  
279 the KPF is dominated by similar ferruginous laminites (**Fig. 9 D**): these contain delicate  
280 flame structures, soft-sediment folds, and are interrupted by granite-rich pebble trains and  
281 rare m-size boulders. The upper part of the KPF is very intermittently exposed but is  
282 characterised by stacked, normally-graded beds of arkosic granular conglomerate, sandstone  
283 and siltstone. Some of the bedsets are, in turn, arranged into decametre-scale coarsening  
284 upward intervals. The composite thickness of the KPF was estimated at 3600 ft (ca. 1100 m)  
285 by Troxel (1967): however, given the very poor bedding continuity, and difficulty in  
286 measuring true thicknesses in this range, it is possible that this is an over-estimation.

287 The nature of the exposure means that this section must be interpreted with great caution.  
288 Nevertheless, phenomena in common with the Silurian Hills succession further to the east

289 include the dark-colour of the diamictites, which contrasts with all other sections described  
290 above, and the presence of lonestones in heterolithic strata: the deflected laminae beneath the  
291 clasts allow us to interpret them as dropstones. Unfortunately, in all other respects, the  
292 fragmentary data (no palaeocurrent information, low resolution logs, discontinuous exposure)  
293 generally preclude us from integrating this substantial outcrop into a regional model.

294

### 295 *The Panamint Range*

296 Although at the time of writing (2017), none of the authors have worked on the Panamint  
297 Range in detail, we summarise the detailed work of others for completeness as it contains the  
298 third thickest section of the KPF in the Death Valley area (after the Kingston Range and the  
299 Silurian Hills). Much of the region was mapped by Labotka *et al.*, (1980), and the KPF was  
300 differentiated into various members and sub-members by these workers. In ascending  
301 stratigraphic order, these units are the Limekiln Spring, Surprise and Sourdough Limestone  
302 members, and the overlying Middle Park and Wildrose sub-members. E-W oriented canyons  
303 dissect the Kingston Peak stratigraphy, and these allowed Miller (1985) to describe the strata  
304 throughout much of the range: the basis of her depositional model. Essentially, regional  
305 correlation has proposed that the Limekiln Spring Formation is equivalent to the unit KP2  
306 diamictite in the eastern Death Valley area, the Surprise Member through Middle Park Sub-  
307 Member correlates to KP3, whereas the Wildrose Diamictite matches with KP4 in the east  
308 (Macdonald *et al.*, 2013).

309 Miller (1983, 1985) established a depositional model in which a northward dipping  
310 palaeoslope was interpreted during deposition of the Limekiln Spring member. Onlap against  
311 crystalline basement to the south of the Goler Wash area was noted earlier (Labotka *et al.*,  
312 1980), with normal faults downstepping to the north. Large blocks of material were described  
313 in diamictites of the latter canyon, and cited as evidence for slope collapse and olistostrome  
314 generation during regional rifting (Prave, 1999). The Goler Wash sections also exhibit  
315 spectacular diamictites that bear close comparison to the boulder-bearing diamictites  
316 described by Le Heron *et al.* (2017) in the Silurian Hills (**Fig. 10 A**). They attain several  
317 hundred metres in thickness. Basalts with a MORB-type composition in the Surprise Member  
318 (Labotka *et al.*, 1980) imply that rift-related tectonic processes played a key role in the  
319 generation of the regional slope in this area (Pettersen *et al.*, 2011). Some possible, albeit  
320 faint, outlines of pillow lava geometries can be observed in Pleasant Canyon (**Fig. 10 B**).

321 Overall, the work of Miller (1985) is made all the more remarkable owing to the degree of  
322 deformation and metamorphism in the southern and central part of the range. However, given  
323 the recent re-interpretation of igneous intrusions as olistoliths in the Silurian Hills KPF  
324 (Vandyk et al., 2018), along with the very limited geochemical dataset available for these  
325 metamorphosed Panamint basalts (Hammond, 1983), it is suggested that these sections now  
326 urgently need re-evaluation to determine whether the metabasites in the Panamints are  
327 actually lavas rather than remobilised slabs of older igneous rocks. Miller (1985) deduced  
328 that northward thickening from 40 m to > 1000 m in this member, in concert with downtract  
329 facies changes from diamictite to greywacke and pelites, lent support to the interpretation of a  
330 north-sloping shelf. She interpreted the diamictite as a lodgement till or glaciomarine deposit,  
331 and the greywackes as turbidites.

332

### 333 **A tale of two rift shoulders, and two ice masses**

334 There are multiple lines of evidence that the Death Valley area was a rifted glaciated margin during  
335 deposition of the KPF. These lines of evidence are outlined below, and then expanded upon in detail  
336 in the following section. The Death Valley area serves as an exemplar for the delivery of material to a  
337 rifted basin from two rift shoulders via two different ice masses, producing markedly contrasting  
338 stratigraphy in the various outcrop belts.

339

#### 340 *The rift margins*

341 Troxel (1966, 1982) made the powerful observation that a northern facies and a southern  
342 facies could be recognised from clast content. In the northern facies, carbonate clasts derived  
343 from underlying units such as the Crystal Spring and Beck Spring formations are  
344 predominant, whereas in the southern facies, crystalline basement lithotypes (notably gneiss,  
345 schist, metabasite, granitoid and quartzite) are much more common (Troxel 1966, 1982).  
346 Different source areas are hence implied, and in palaeogeographic terms, two upland areas  
347 were posited as source areas for the clasts: a Mojave Upland which drained to the north, and a  
348 Nopah Upland which drained in approximately the opposite direction toward the south  
349 (Wright *et al.*, 1974). The existence of opposing palaeoslopes was strong circumstantial  
350 evidence for the presence of a failed rift running approximately E-W and occupied by the  
351 present day Amargosa canyon: the Amargosa aulacogen (Wright *et al.*, 1974). Palaeocurrent



352 analysis supports the concept of northern and southern source areas (e.g. Le Heron and  
353 Busfield, 2016). These source areas reflect the delivery of material from two upland regions  
354 (to the present day north and to the present day south). As will be shown below, these upland  
355 regions correspond to two rift shoulders.

356 Whilst the concept of an aulacogen in the Amargosa area has subsequently fallen out  
357 of favour (see Mahon *et al.*, 2014), strong evidence for rifting during Kingston Peak time  
358 remains. Critical to this interpretation are intercalated MORB-type pillow lavas (Hammond,  
359 1983) in the Panamint Range on the western Death Valley flank (Labotka *et al.*, 1980), within  
360 the so-called Surprise Member (Miller, 1985). Furthermore, en echelon growth faults in the  
361 Kingston Range are interpreted as the signature of a rift margin (Walker *et al.*, 1986). This  
362 extensional fault array is known to have been the source area for megaclasts (Terry and Goff,  
363 2014) within the KPF (Le Heron, 2015). The major lateral thickness variations across the  
364 Death Valley area are also compatible with rift-generated accommodation space (Prave,  
365 1999).

366

### 367 *Converging ice masses*

368 Although northern and southern source areas can be distinguished by clast content (Troxel,  
369 1966), in practice the effects of Cenozoic strike-slip tectonics has produced a major challenge  
370 for any meaningful palaeo-ice sheet reconstruction. The most continuous outcrop belt lies in  
371 the Panamint Range immediately west of Death Valley (**Fig. 1**), where metasedimentary  
372 rocks extend for up to 100 km from N-S, locally reaching amphibolite facies. The presence of  
373 two ice centres in the Panamint Range seems likely, in the Goler Wash area to the south and  
374 on the so-called World Beater dome further north (Miller, 1985; Prave, 1999). Yet it remains  
375 highly uncertain how, if at all, these ice masses connected with those in the eastern Death  
376 Valley area, and substantial additional work is required to resolve this issue. Outcrops of  
377 much lower quality occur elsewhere, including the Black Mountains at the eastern flank of  
378 Death Valley. In terms of a regional picture, on the basis of detrital zircon analysis and  
379 provenance studies, the Death Valley area could be posited to be a regional basin during KPF  
380 time, thus receiving sediment from all sides and not just the north and south (Mahon *et al.*,  
381 2014b).

382

383 In spite of the Cenozoic tectonic overprint noted above, Le Heron and Busfield (2016) were  
384 able to propose a palaeogeographic reconstruction and ice sheet reconstruction for a small  
385 area of eastern Death Valley, encompassing the Kingston Range, Sperry Wash and Silurian  
386 Hills areas (**Fig. 1 B**). A grounding zone was recognised in the Sperry Wash area on account  
387 of a thick diamictite with delicately intercalated soft-sediment deformation interpreted as  
388 glaciotectonic structures (Busfield and Le Heron, 2016), and a fjordal setting was suggested.  
389 This area was viewed as proximal to much of the Kingston Range, with identical (SE-  
390 directed) palaeocurrents measured from medial and distal turbidite sandstones throughout the  
391 succession (Le Heron et al., 2018). All of these areas are dominated by carbonate clasts and  
392 detritus. By contrast, the completely different character of the Silurian Hills succession, being  
393 dominated by crystalline basement detritus and exhibiting N-directed palaeocurrents (Basse,  
394 1980) underscores the idea of provenance from a separate ice mass. The glaciogenic affinity  
395 of the diamictites in the Silurian Hills area has subsequently been demonstrated (Le Heron et  
396 al., 2017).

397

#### 398 **The case for diachronous rifting and diachronous glaciation**

399 The recent discovery of dropstones in both the Silurian Hills (Le Heron et al., 2017) and in  
400 the Salt Spring Hills, the latter presented for the first time herein, is very significant because  
401 it provides affirmation that the KPF is indeed present at the expected stratigraphic levels. For  
402 example, given the presence of cobble-bearing diamictites in strata beneath the KPF in the  
403 Silurian Hills (interpreted as fluvial deposits: Basse, 1978), miscorrelation is clearly possible.  
404 Thus, the presence of dropstones set the scene for testing models that promote the  
405 interpretation of regionally extensive stratigraphic units of the KPF.

406 In the Kingston Range, Walker *et al.* (1986) interpreted evidence for syn-depositional  
407 extension from within the KPF near Horsethief Springs. In map view (**Fig. 11 A, B**),  
408 evidence for growth strata includes the thickening of units onto hanging-wall blocks in the  
409 north of that range. From a global perspective, Eyles and Januszczak (2004) posited that  
410 Cryogenian glaciation occurred diachronously, with ice sheets selectively populating the rift  
411 shoulders of an unzipping Rodinia supercontinent. Their model cautioned that  
412 lithostratigraphic correlation of Cryogenian diamictites may not take into account the  
413 expected diachroneity, a point also made in age compilations for Neoproterozoic diamictites  
414 by Allen and Etienne (2008) and Spence et al. (2016). At the scale of Death Valley, it has

415 been proposed that the diamictite-bearing units can be correlated between many of the  
416 constituent outcrop belts (e.g. between the Kingston Range, the Saddle Peak Hills, the  
417 Silurian Hills and the Panamints) (Prave, 1999), with later work advocating that they are  
418 essentially chronostratigraphic markers that form the basis of tectonostratigraphic units across  
419 the north American Cordillera (Macdonald *et al.*, 2013). Noting this, Le Heron *et al.* (2017)  
420 questioned the validity of this claim because at least four diamictite intervals of glacial origin  
421 in the Silurian Hills (**Fig. 2 D**, **Fig. 11 C**), representing at least four localised pulses of  
422 glaciation, were proposed in that paper. These glacial diamictites are intercalated with at least  
423 four olistostrome intervals which contain obvious 30-100 m wide carbonate megaclasts (**Fig.**  
424 **11 D, E**). This stratigraphic record differs substantially from that in the southern Kingston  
425 Range, where a lower and an upper diamictite are recognised (Le Heron *et al.*, 2018),  
426 sandwiching a single olistostrome. Even the most basic comparison between the logs (**Fig. 2**  
427 **C, D**) identifies major differences in stratigraphy in these study areas, which may result from  
428 diachroneity of glacial sediment input, in conjunction with asynchronous activation of basin-  
429 bounded faults which might be expected in a rift system. Here, we propose that the different  
430 stratigraphy in the Silurian Hills and in the Kingston Range can simply be explained by  
431 separate ice masses feeding separate minibasins in an evolving rift system. This model  
432 acknowledges both the strong glacial control on sedimentation, and the rifting context,  
433 explaining why diamictites cannot be correlated from one outcrop belt to another.  
434 Neighbouring ranges preserve different stratigraphy because they represent different  
435 minibasins in the rift system, explaining not only the dramatic thickness variations from  
436 range to range, but also the number of olistostromes (if present) in each range.

437 Vandyk *et al.* (2018) examined metabasite igneous bodies in the Silurian Hills which  
438 were previously mapped and interpreted as sills (Kupfer, 1960; Basse, 1978). In summary,  
439 metabasite bodies in both the Kingston Range and in the Silurian Hills were found to yield U-  
440 Pb apatite ages of approximately 1.1 Ga, which are remarkably close in age to the 1.05 Ga  
441 diabase intrusions in the underlying Crystal Spring Formation (Heaman and Grotzinger,  
442 1992). Based on geochemical arguments, in conjunction with evidence for disaggregated  
443 blocks of metabasite within the diamictites, a revised interpretation of elongate, bedding  
444 parallel metabasite olistoliths was proposed. These new interpretations challenged the  
445 conventional wisdom on syn-glacial magmatism in the eastern Death Valley area. Given this,  
446 they raise regional questions about the degree of magma production during glaciation, and  
447 indeed whether long described pillow basalts in diamictites in the Surprise Member in the

448 Panamint Range (west of Death Valley) (Labotka *et al.*, 1980; Miller, 1985) were emplaced  
449 onto a glaciated sea floor or whether these, too, are olistoliths of older basaltic material.  
450 Stratigraphic models through the succession in the Panamint Range (**Fig. 11 F**) certainly  
451 suggest that this hypothesis demands further investigation.

452 In spite of the complexities outlined above, two patterns emerge: (i), there is excellent  
453 evidence for glacial processes recorded in almost all of the outcrop belts of the KPF and (ii),  
454 facies variations, and stratigraphic stacking patterns, are sufficiently dramatic to question  
455 assertions that tectonostratigraphic units can be confidently identified. Regarding the first  
456 point, new data from the Salt Spring Hills allow excellent dropstones to be recognised for the  
457 first time. With regard to the second issue, tentative palaeogeographic maps (**Fig. 1**) precis  
458 this problem: it is unsurprising that convergent ice masses, from opposite source areas,  
459 produce different stacking patterns, and it is unsurprising that at the local scale these ice  
460 masses may have behaved diachronously. It should be noted that the complete lack of  
461 *absolute* geochronological control on the KPF *does not* mean that the idea of broadly  
462 synchronous ice masses feeding the basin(s) should be dismissed immediately. Within the  
463 framework of a synchronous glaciation, it is possible that neighbouring glaciers advance and  
464 retreat slightly out of phase. However, observation of modern valley glaciers in Nepal, for  
465 example, demonstrates synchronous patterns of retreat in response to climate forcing  
466 (Bajracharya and Mool, 2009). In combination, the issues discussed above make attempts to  
467 assign tectonostratigraphic significance to the diamictite strata premature at present,  
468 especially considering that the only absolute age dates from the strata appear to derive from  
469 olistoliths (Vandyk *et al.*, 2018), although it should be acknowledged that excellent detrital  
470 zircon data are available (Mahon *et al.*, 2014a, b). Thus, the rocks await considerable and  
471 continued work to gain a fuller picture of the Neoproterozoic rifted glaciated margin of Death  
472 Valley, California.

473

## 474 **Conclusions**

- 475 • Evidence for glaciation in the KPF is excellent throughout the eastern Death Valley  
476 area, with the presence of unequivocal dropstones leaving no doubt that the KPF can  
477 be correlated as a unit. Their recent discovery in locations such as the Salt Spring  
478 Hills and the Silurian Hills (Le Heron *et al.*, 2017) considerably extends the “proven”  
479 extent of the glaciogenic facies;

480  
481  
482  
483  
484  
485  
486  
487  
488  
489  
490  
491  
492  
493  
494  
495  
496  
497  
498  
499  
500  
501  
502  
503  
504  
505

- In general terms, a setting of subaqueous, glaciogenic debris flows, feeding glaciomarine turbidites is envisaged across the region, with dropstones advected through ice rafting. Set against a probable fjordal setting, a picture of two ice sheets flowing from north to south (the Nopah ice sheet) and from south to north (the Mojave ice sheet) emerges, and sets the context for Cryogenian glaciation in this area. The relationship of ice masses between the Panamint Range and the eastern Death Valley outcrops remains conjectural and requires substantial further work;
- Basic comparison of the thickest sections of the KPF in the type area (Kingston Range) and in the Silurian Hills underscores how difficult it is to correlate this formation between neighbouring ranges. With this in mind, and in the absence of any absolute age constraints for the KPF, arguments for regional chronostratigraphic units are premature. It is equally likely that the individual diamictites were deposited diachronously across the different ranges;
- In most ranges, the sedimentary record demonstrates that that glacial input and non-glacial processes (slope failure) vied for stratigraphic supremacy. Evidence for syn-sedimentary faulting during deposition of the KPF is recognised in three outcrop belts, namely the Kingston Range, the Silurian Hills, and in the Panamint Range, upholding the long-held view of rifting superimposed on glaciation, or vice-versa. We propose a model for the regional accumulation of the KPF whereby glacial and non-glacial (slope) diamictites accumulated together in rift-shoulder minibasins, producing locally contrasting stratigraphy. This model stands in stark contrast to previous work that viewed the individual diamictites as regional chronostratigraphic units.

## 506 **Acknowledgments**

507 We are very grateful to the Geological Society of London for multiple grants from 2012 to  
508 2016 that has supported five field seasons in the Death Valley area and multiple research  
509 projects of our group. We are thankful to the two anonymous reviewers who provided some  
510 excellent suggestions for improvement. We also acknowledge excellent discussions about the  
511 KPF and Death Valley geology in general from Professor Tony Prave, Professor Darrel  
512 Cowan, Professor Carol Dehler. We could not conclude without acknowledging Cynthia  
513 Kienetz for her outstanding hospitality, friendship and accommodation in Tecopa.

514

515 **References**

- 516 ALLEN, P.A. & ETIENNE, J.L. 2008. Sedimentary challenge to snowball Earth. *Nature*  
517 *Geoscience*, **1**, 817–825.
- 518 BAJRACHARYA, S.R. & MOOL, P. 2009. Glaciers, glacial lakes and glacial lake outburst floods  
519 in the Mount Everest region, Nepal. *Annals of Glaciology* **50**, 81-86.
- 520 BASSE, R.A. 1978. Stratigraphy, Sedimentology and Depositional Setting of the Late  
521 Precambrian Pahrump Group, Silurian Hills, California. MS Thesis, Stanford University,  
522 86p.
- 523 BUSFIELD, M.E. & LE HERON, D.P. 2016. A Neoproterozoic ice advance sequence, Sperry  
524 Wash, California. *Sedimentology*, **63**, 307–330.
- 525 BUSFIELD, M.E. & LE HERON, D.P. 2018. Snowball Earth under the microscope. *Journal of*  
526 *Sedimentary Research*.
- 527 CALZIA, J.P., TROXEL, B.W., WRIGHT, L.A., BURCHFIEL, B.C., DAVIS, G.R., McMACKIN,  
528 M.R. 2000. Geologic map of the Kingston Range, southern Death Valley, California. *USGS*  
529 *Open File Report 2000-412*.
- 530 CREVELING, J.R., BERGMANN, K.D. & GROTZINGER, J.P., 2016. Cap carbonate platform facies  
531 model, Noonday Formation, SE California. *Geol. Soc. Am. Bull.* **128** (7–8), 1249–1269.
- 532 EYLES, N., & JANUSZCZAK, N. 2004. ‘Zipper-rift’: A tectonic model for Neoproterozoic  
533 glaciations during the breakup of Rodinia after 750 Ma. *Earth-Science Reviews*, **65**, 1-73.
- 534 FRIDRICK, C.J. & THOMPSON, R.A. 2011. Cenozoic Tectonic Reorganizations of the Death  
535 Valley Region, Southeast California and Southwest Nevada. *U.S. Geological Survey*  
536 *Professional Paper 1783*, 36 p. and 1 plate.
- 537 GUEST, B., PAVLIS, T.L., GOLDING, H. & SERPA, L. 2003. Chasing the Garlock: A study of  
538 tectonic response to vertical axis rotation. *Geology*, **31**, 553-556.
- 539 HAMMOND, J.L.G., 1983. Late Precambrian diabase intrusions in the southern Death Valley  
540 region, California: Their petrology, geochemistry, and tectonic significance. PhD thesis,  
541 University of Southern California.
- 542 HEAMAN, L.M. & GROTZINGER, J.P. 1992. 1.08 Ga diabase sills in the Pahrump Group,  
543 California: implications for development of the Cordilleran miogeocline. *Geology*, **20**, 637–  
544 640.
- 545 HOFFMAN, P.F. & SCHRAG, D.P. 2002. The snowball Earth hypothesis: testing the limits of  
546 global change. *Terra Nova*, **14**, 129-155.

- 547 HOFFMAN, P.F. ABBOT, D.S., ASHKENAZY, Y., BENN, D.I., BROCKS, J.J., COHEN, P.A., COX,  
548 G.M., CREVELING, J.R., DONNADIEU, Y., ERWIN, D.H., FAIRCHILD, I.J., FERREIRA, D.,  
549 GOODMAN, J.C., HALVERSON, G.P., JANSEN, M.J., LE HIR, G., LOVE, G.D., MACDONALD,  
550 F.A., MALOOF, A.C., PARTIN, C.A., RAMSTEIN, G., ROSE, B.E.J., ROSE, C.V., SADLER, P.M.,  
551 TZIPERMAN, E., VOIGT, A., & WARREN, S.G. 2017. Snowball Earth climate dynamics and  
552 Cryogenian geology-geobiology. *Science Advances* 3, E1600983. DOI:  
553 10.1126/SCIADV.1600983
- 554 KUPFER, D.H. 1960. Thrust faulting and chaos structure, Silurian Hills, San Bernadino  
555 County, California. *GSA Bulletin*, **71**, 181-214.
- 556 LABOTKA, T.C., ALBEE, A.L., LANPHERE, M.A. & MCDOWELL, S.D. 1980. Stratigraphy,  
557 structure and metamorphism in the central Panamint Mountains (Telescope Peak  
558 quadrangle), Death Valley area, California, *Geological Society of America Bulletin*, **91**,  
559 843–933.
- 560 LE HERON, D.P. 2015. The significance of ice-rafted debris in Sturtian glacial successions.  
561 *Sedimentary Geology*, **322**, 19-33.
- 562 LE HERON, D.P. & BUSFIELD, M.E. 2016. Pulsed iceberg delivery driven by Sturtian ice sheet  
563 dynamics: An example from Death Valley, California. *Sedimentology*, **63**, 331-349.
- 564 LE HERON, D.P., BUSFIELD, M.E. & PRAVE, A.R. 2014. Neoproterozoic ice sheets and  
565 olistoliths: multiple glacial cycles in the Kingston Peak Formation, California. *Journal of*  
566 *the Geological Society, London*, **171**, 525–538.
- 567 LE HERON, D.P., TOFAIF, S., VANDYK, T., ALI, D.O. 2017. A diamictite dichotomy: Glacial  
568 conveyor belts and olistostromes in the Neoproterozoic of Death Valley, California, USA.  
569 *Geology*, **45**, 31-34.
- 570 LE HERON, D.P., BUSFIELD, M.E., ALI, D.O., AL TOFAIF, S. & VANDYK, T.M. 2018. The  
571 Cryogenian record in the southern Kingston Range, California: The thickest Death Valley  
572 succession in the hunt for a GSSP. *Precambrian Research*,  
573 <http://dx.doi.org/10.1016/j.precamres.2017.07.017>
- 574 LEVY, M. & CHRISTIE-BLICK, N. 1989. Pre-Mesozoic Palinspastic Reconstruction of the  
575 Eastern Great Basin (Western United States). *Science*, **245**, 1454-1462.
- 576 MACDONALD, F.A., PRAVE, A.R., PETTERSON, R., SMITH, E.F., PRUSS, S.B., OATES, K.,  
577 TROTZUK, D. & FALICK, A.E. 2013. The Laurentian record of Neoproterozoic glaciation,  
578 tectonism, and eukaryotic evolution in Death Valley, California. *Geological Society of*  
579 *America Bulletin*, **125**, 1203–1223.
- 580 MAHON, R.C., DEHLER, C.M., LINK, P.K., KARLSTROM, K.E. & GEHRELS, G.E. 2014a.  
581 Geochronologic and stratigraphic constraints on the Mesoproterozoic and Neoproterozoic  
582 Pahump Group, Death Valley, California: A record of the assembly, stability, and  
583 breakup of Rodinia. *Geological Society of America Bulletin*, **126**, 652-664.

- 584 MAHON, R.C., DEHLER, C.M., LINK, P.K., KARLSTROM, K.E. & GEHRELS, G.E. 2014b. detrital  
585 zircon provenance and paleogeography of the Pahrump Group and overlying strata, Death  
586 Valley, California. *Precambrian Research*, **251**, 102-117.
- 587 MILLER, J.M.G. 1983. Stratigraphy and sedimentology of the upper Proterozoic Kingston  
588 Peak Formation, Panamint Range, eastern California. PhD Thesis, Santa Barbara,  
589 California, University of California, 335 pp.
- 590 MILLER, J.M.G. 1985. Glacial and syntectonic sedimentation: The upper Proterozoic  
591 Kingston Peak Formation, southern Panamint Range, eastern California. *Geological*  
592 *Society of America Bulletin*, **96**, 1537-1553.
- 593 MROFKA, D. 2010. Competing models for the timing of Cryogenian Glaciation: Evidence  
594 from the Kingston Peak Formation, southeastern California. PhD dissertation, University  
595 of California, Riverside.
- 596 MROFKA, D. & KENNEDY, M. 2011. The Kingston Peak Formation in the eastern Death  
597 Valley region. In: ARNAUD, E., HALVERSON, G.P. & SHIELDS-ZHOU, G. (eds) *The*  
598 *Geological Record of Neoproterozoic Glaciations*. Geological Society, London,  
599 *Memoirs*, **36**, 449-458.
- 600 PETTERSON, R., PRAVE, A.R. & WERNICKE, B.P. 2011. Glaciogenic and related strata of the  
601 Neoproterozoic Kingston Peak Formation in the Panamint Range, Death Valley region,  
602 California. In: *The Geological Record of Neoproterozoic Glaciations* (Eds E. Arnaud, G.P.  
603 Halverson and G. Shields-Zhou). Geological Society, London, *Memoirs*, **36**, 449-458.
- 604 PRAVE, A.R. 1999. Two diamictites, two cap carbonates, two  $\delta^{13}\text{C}$  excursions, two rifts: the  
605 Neoproterozoic Kingston Peak Formation, Death Valley, California. *Geology*, **27**, 339-  
606 324.
- 607 SPENCE, G.H., LE HERON, D.P., & FAIRCHILD, I.J. 2016, Sedimentological perspectives on  
608 climatic, atmospheric and environmental change in the Neoproterozoic Era.  
609 *Sedimentology*, **63**, 253–306.
- 610 TERRY, J.P. & GOFF, J. 2014. Megaclasts: proposed revised nomenclature at the coarse end of  
611 the Udden-Wentworth grain-size scale for sedimentary particles. *Journal of Sedimentary*  
612 *Research*, **84**, 192-197.
- 613 TROXEL, B.W. 1966. Sedimentary Features of the Later Precambrian Kingston Peak  
614 Formation, Death Valley. *Geological Society of America Special Paper* **101**, California  
615 341 p.
- 616 TROXEL, B.W. 1967. Sedimentary rocks of the Late Precambrian and Cambrian age in the  
617 southern Salt Spring Hills, southeastern Death Valley, California. *California Division of*  
618 *Mines and Geology*, **SR92**, 33-41.
- 619 TROXEL, B.W. 1982, Description of the uppermost part of the Kingston Peak Formation,  
620 Amargosa Rim Canyon, Death Valley region, California. In: COOPER, J.D., TROXEL, B.W.,



621 & WRIGHT, L.A. (eds), *Geology of Selected Areas in the San Bernardino Mountains,*  
622 *Western Mojave Desert, and Southern Great Basin, California: Volume and Guidebook for*  
623 *Field Trip No. 9, 78<sup>th</sup> Anniversary Meeting of Cordilleran Section, Geological Society of*  
624 *America. Shoshone, California, Death Valley Publishing Company, 61–70.*

625 VANDYK, T.M., LE HERON, D.P., CHEW, D.M., AMATO, J.M., THIRLWALL, M., DEHLER,  
626 HENNIG, J., CASTONGUAY, S.R., KNOTT, T., TOFAIF, S., ALI, D.O., MANNING, BUSFIELD,  
627 M.E., DOEPKE, D. & GRASSINEAU, N. 2018. Precambrian olistoliths masquerading as sills  
628 from Death Valley, California. *Journal of the Geological Society, London.*  
629 <https://doi.org/10.1144/jgs2017-002>

630 WALKER, J.D., KLEPACKI, D.W., & BURCHFIEL, B.C. 1986. Late Precambrian tectonism in the  
631 Kingston Range, southern California: *Geology*, **14**, 15–18.

632 WRIGHT, L.A., TROXEL, B.W., WILLIAMS, E.G., ROBERTS, M.T. & DIEHL, P.E. 1974.  
633 Precambrian sedimentary environments of the Death Valley region, eastern California and  
634 Nevada. In: *Geological Society of America, Guidebook: Death Valley region, California*  
635 *and Nevada* [prepared for the 70th Annual Meeting of Cordilleran Section, Geological  
636 Society of America]. The Death Valley Publishing Company, Shoshone, CA, 27–35.

637

638

### 639 **Figure captions**

640 *Figure 1:* A: Location of Death Valley in the Basin and Range province, with location of the  
641 six study areas referred to in this paper indicated. B: Palaeogeographic reconstructions of the  
642 eastern Death Valley area during deposition of the Kingston Peak Formation, based upon  
643 integration of data from the Kingston Range, Sperry Wash and Silurian Hills areas. Modified  
644 from Le Heron & Busfield (2016).

645 *Figure 2:* Sedimentary logs of the Kingston Peak Formation from four separate ranges in the  
646 eastern Death Valley region. A: Sperry Wash, modified and simplified after Busfield & Le  
647 Heron (2016). B: Saddle Peak Hills, reproduced at high resolution- a previously unpublished  
648 partial section of a high quality, but intensely faulted, succession. C: Silurian Hills, modified  
649 from Le Heron et al. (2017). D: Southern Kingston Range- a previously unpublished section.  
650 Note that the scale bars on each of the logs: C and D are coarse resolution logs shown at the  
651 same scale as each other for direct comparison.

652 *Figure 3:* Representative sedimentary facies of the Sperry Wash area. A: General view  
653 showing well-bedded nature of the strata. Prominent ridges are composed of conglomerate.  
654 B: Channelised conglomerate, cutting down into ferruginous shales. C: Classic normally-  
655 graded bed of conglomerate, fining up to medium-grained sandstone. D: Large outsized clast  
656 of dolostone encased in mudstone deflecting underlying layers. E: Dm-thick diamictite  
657 encased in siltstone. F: Intensely deformed interval of laminites, interpreted as a  
658 glacitectorite (Busfield & Le Heron, 2016). G: Intricate ball and pillow structures. H:

659 Stratified diamictite interpreted as sub-ice shelf rainout deposits (Busfield & Le Heron,  
660 2016).

661 *Figure 4:* Representative sedimentary facies in the Saddle Peak Hills range. A: Beck Spring  
662 Dolomite directly overlain by the Kingston Peak Formation. Strata are dipping northward  
663 (i.e. into the page) at about 25°. B: Ferruginous siltstones with thin graded sandstone beds  
664 sharply overlain by a thick, normally-graded conglomerate bed. Note hammer (30 cm long)  
665 for shale. C: Detail of diamictite, with abundant carbonate clasts derived from the underlying  
666 Beck Spring Dolomite. D: Classic normally-graded beds (more prominent horizons)  
667 punctuating more recessive, stratified siltstones. E: Lonestone of dolostone within stratified  
668 silty shale. F: Graded sandstone bed overlain by lonestone-bearing silty shale.

669 *Figure 5:* Kingston Peak facies in the Kingston Range area. A: Interbedded sandstones and  
670 siltstones which dominate much of the upper part of the formation above the olistostrome  
671 complex. B: Detail of a graded bed, interpreted as a turbidite (Le Heron et al., 2014): typical  
672 of the supra-olistostrome strata. C: Dropstone of Beck Spring Dolomite loading ferruginous  
673 shales. D: Rhythmically bedded siltstones and fine-grained sandstone, punctuated by small  
674 pebbles (dropstones). E: Diamictite toward the top of the Kingston Peak Formation, cropping  
675 out with typical low-lying exposure. F: Stratified diamictite with a quartzite dropstone toward  
676 the very top of the Kingston Peak Formation, about 10 m below the unconformity with the  
677 overlying Noonday Dolomite. G: Polished pebble in the diamictite. H: Possible striations on  
678 the surface of the striated pebble.

679 *Figure 6:* A: Typical outcrop of massive diamictite in the Alexander Hills. B: Detail of the  
680 massive diamictite (foliations are tectonic), with characteristically rounded pebbles of  
681 basement lithologies (gneiss, granitoid) and basement cover strata (dolostone, quartzite).

682 *Figure 7:* Kingston Peak facies in the Silurian Hills area. A: Steeply dipping strata  
683 comprising interstratified, boulder-bearing diamictite (to the left of the hammer) and  
684 heterolithic strata (turbidite sandstones and siltstones) to the right of the photo. B: Detail of  
685 typical boulder-bearing diamictite. Each of the visible clasts comprise schist and gneiss. C:  
686 Delicately laminated siltstones and sandstones. D: Quartzite cobble interpreted as a  
687 dropstone, with clear deflection and downwarping of siltstone layers.

688 *Figure 8:* Simple sketch log through part of the succession exposed in the Salt Spring Hills.  
689 To the authors' knowledge, no sedimentary log has previously been published for rocks in  
690 these hills, although Mrofka (2010) records the composition of the diamictites in this range,  
691 noting overall similarities to the Silurian Hills sections. Refer to Fig. 2 for the legend.

692 *Figure 9:* Kingston Peak facies in the southern Salt Spring Hills area. A: Typical outcrop  
693 style, characterised by frustratingly discontinuous layers, although high quality lithological  
694 observations can still be made. B: Structureless / massive diamictite dominated much of the  
695 exposed Kingston Peak succession. C: Exquisite dropstone textures in interstratified siltstone  
696 and fine-grained sandstone. D: Well stratified, ferruginous siltstones and shales with scattered  
697 lonestones toward the middle of the studied section.

698 *Figure 10: Aspects of the Kingston Peak Formation in the Panamint Range. A: Thick*  
699 *accumulation of boulder-bearing diamictites in the Goler Wash area at the southern extremity*  
700 *of the range. B: Metabasite in the Pleasant Canyon section, in the central part of the range,*  
701 *crosscut by serpentinite veins, producing a ghostly “pillow-like” aspect to the exposure.*  
702 *These probably correspond to the MORB basic rocks reported by others (Labotka et al.,*  
703 *1980). C: The Wildrose diamictite in the northern part of the range (Wildrose Canyon)- note*  
704 *attenuated clasts, dominantly of a carbonate composition.*

705 *Figure 11: A and B: Satellite image and geological sketch map of part of the northern part of*  
706 *the Kingston Range exposures (modified from Le Heron et al., 2014), showing en echelon,*  
707 *NE-SW oriented normal fault arrays. Note the thickness changes of the various synglacial*  
708 *units across the faults, and the abrupt termination of some units against the footwall blocks.*  
709 *C: Geological facies map of the Silurian Hills, from Le Heron et al. (2017). Note the*  
710 *mappable megaclasts in this region, and the occurrence of two types of diamictite on the*  
711 *legend: a boulder-bearing diamictite (interpreted to represent glacial material) and a*  
712 *megaclast-bearing diamictite (interpreted to be repeated stratigraphic occurrences of*  
713 *olistostromes) (Le Heron et al., 2017). D and E: Google Earth image, looking south, with*  
714 *corresponding photo of a megaclast-bearing interval (megaclasts are arrowed). F: Sketch*  
715 *cross section through part of the Panamint Range (redrawn from Miller, 1985), showing syn-*  
716 *sedimentary extensional fault system that was active during deposition of the Kingston Peak*  
717 *Formation.*

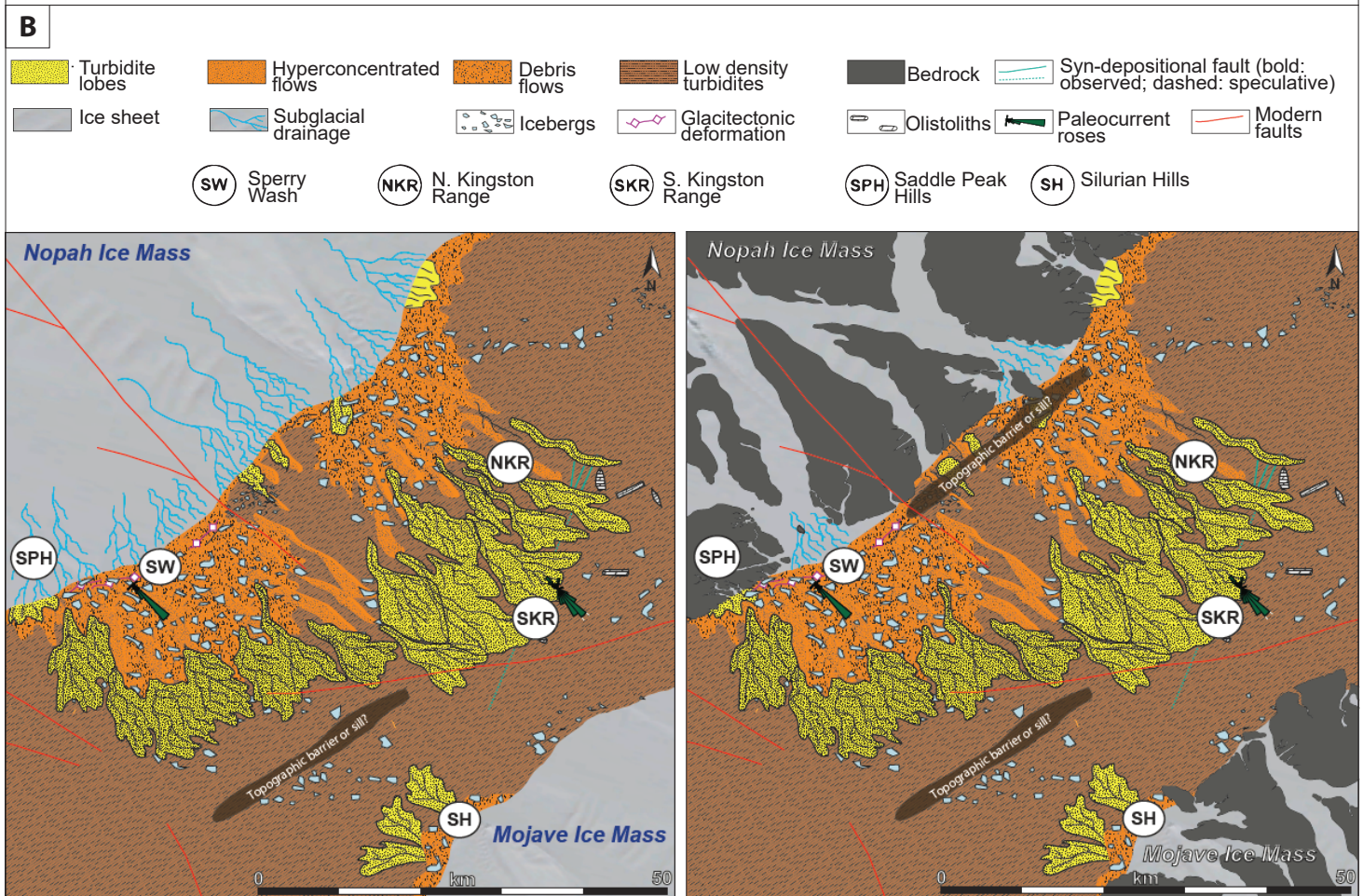
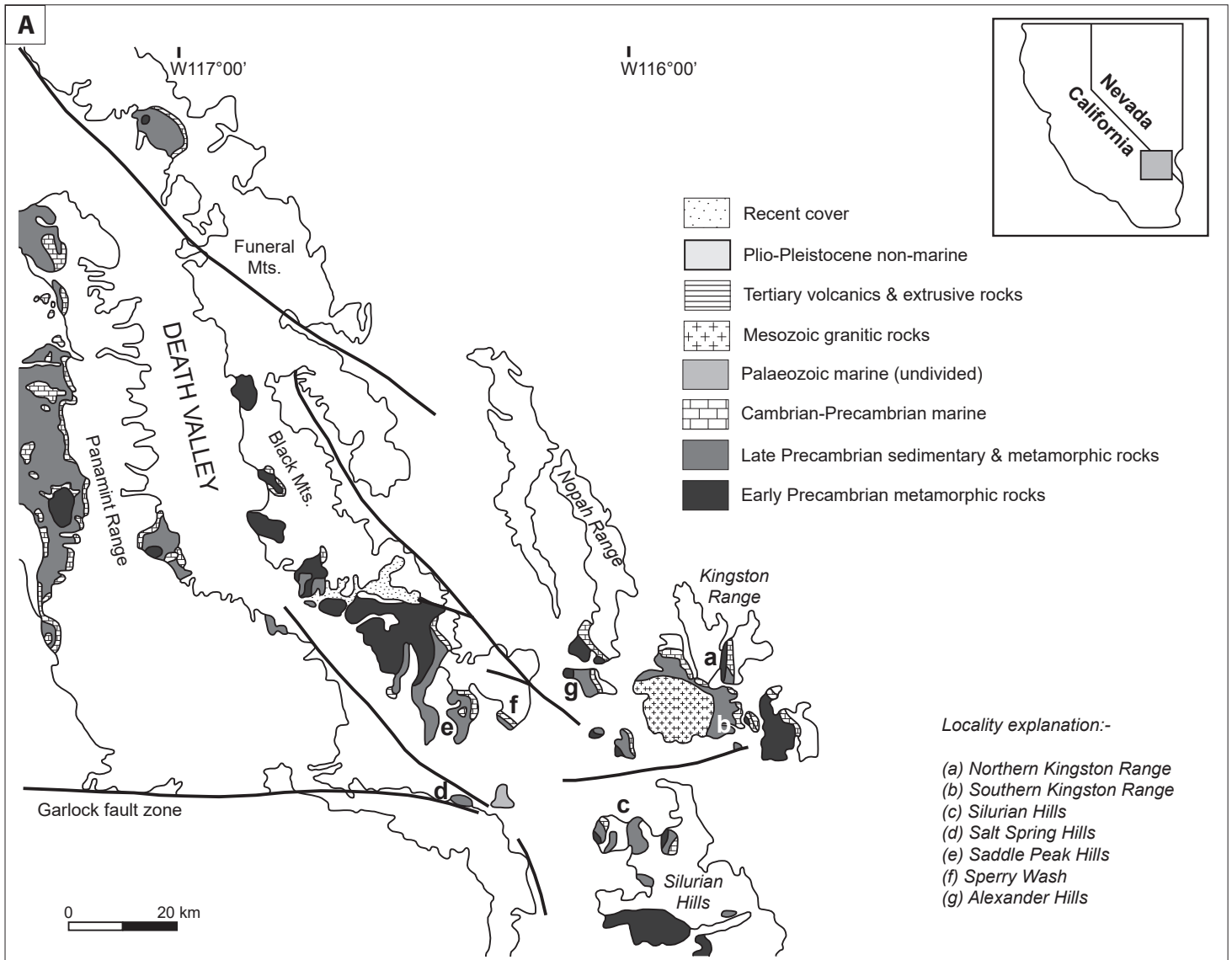


Figure 1



**A: Sperry Wash**

**B: Saddle Peak Hills**

**C: Southern Kingston Range**

**D: Silurian Hills**

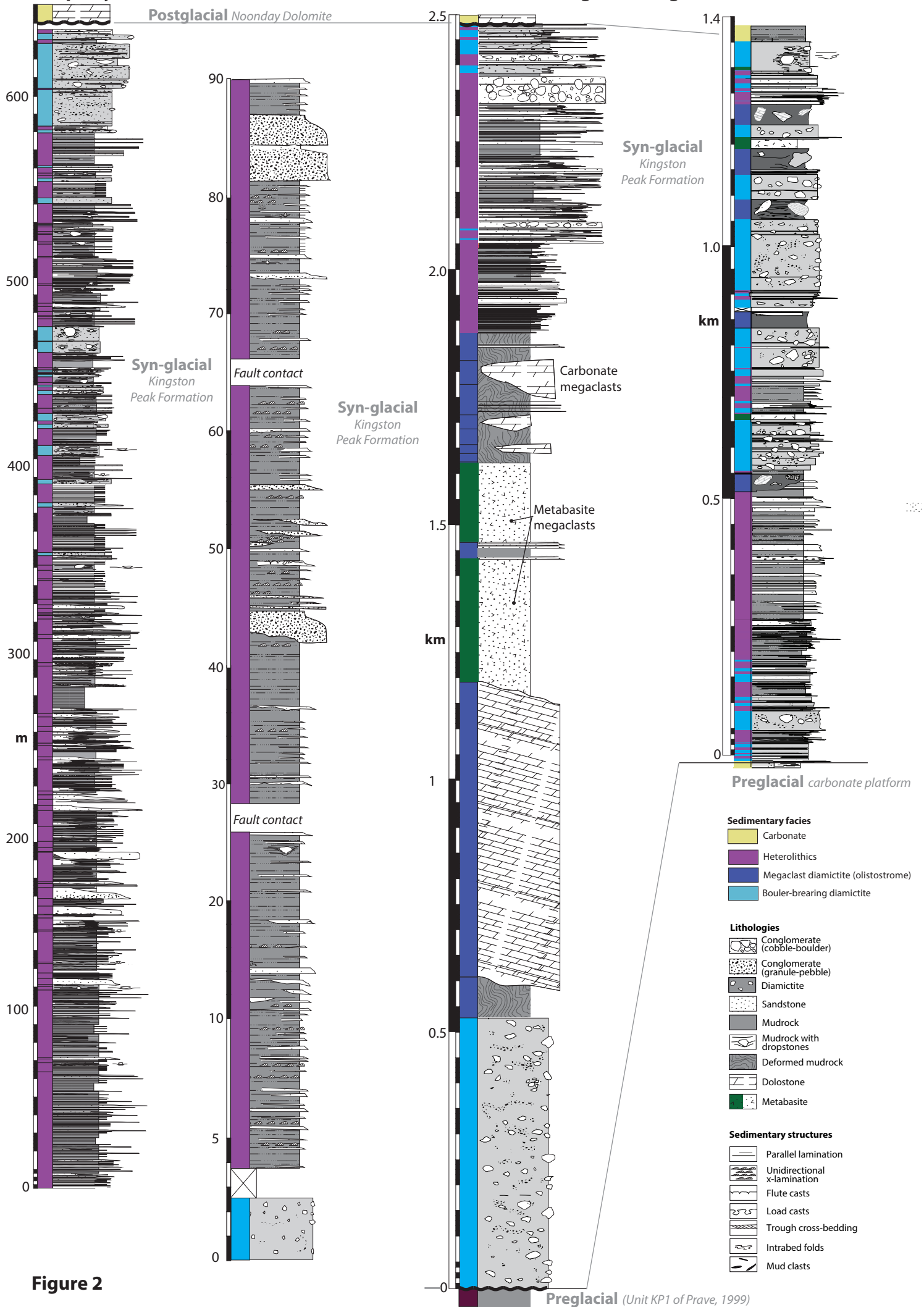


**Figure 2**



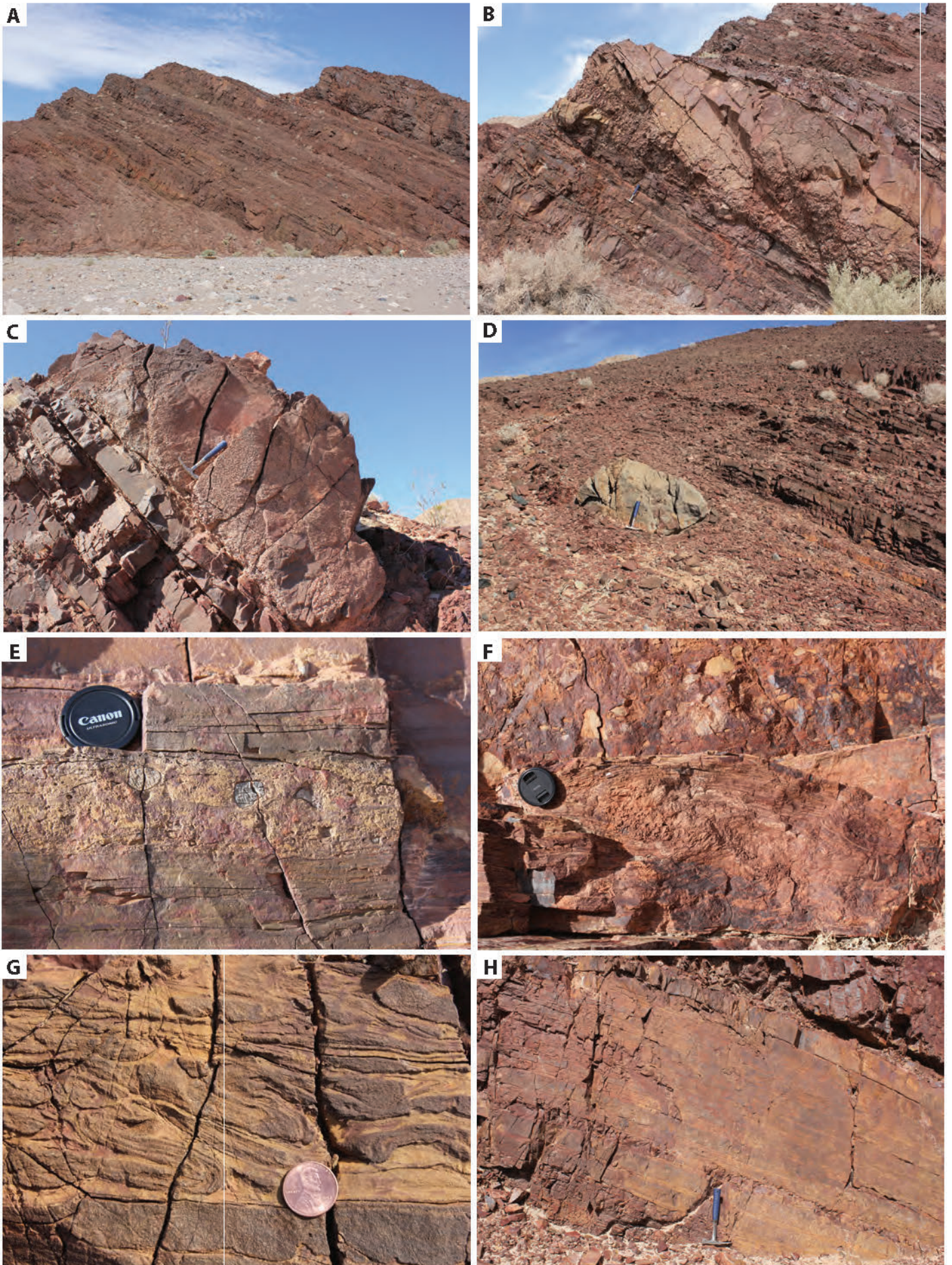


Figure 3



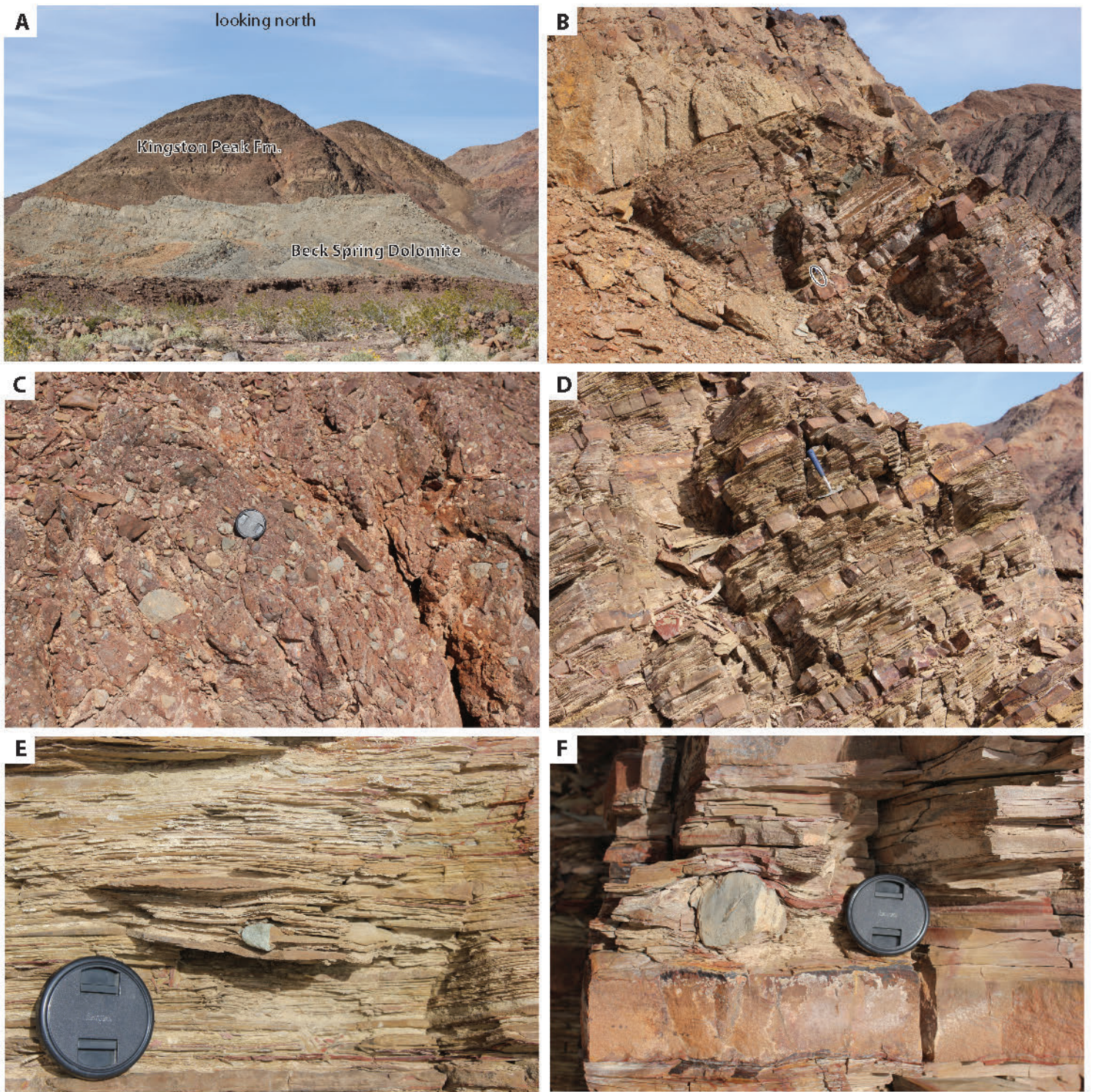


Figure 4



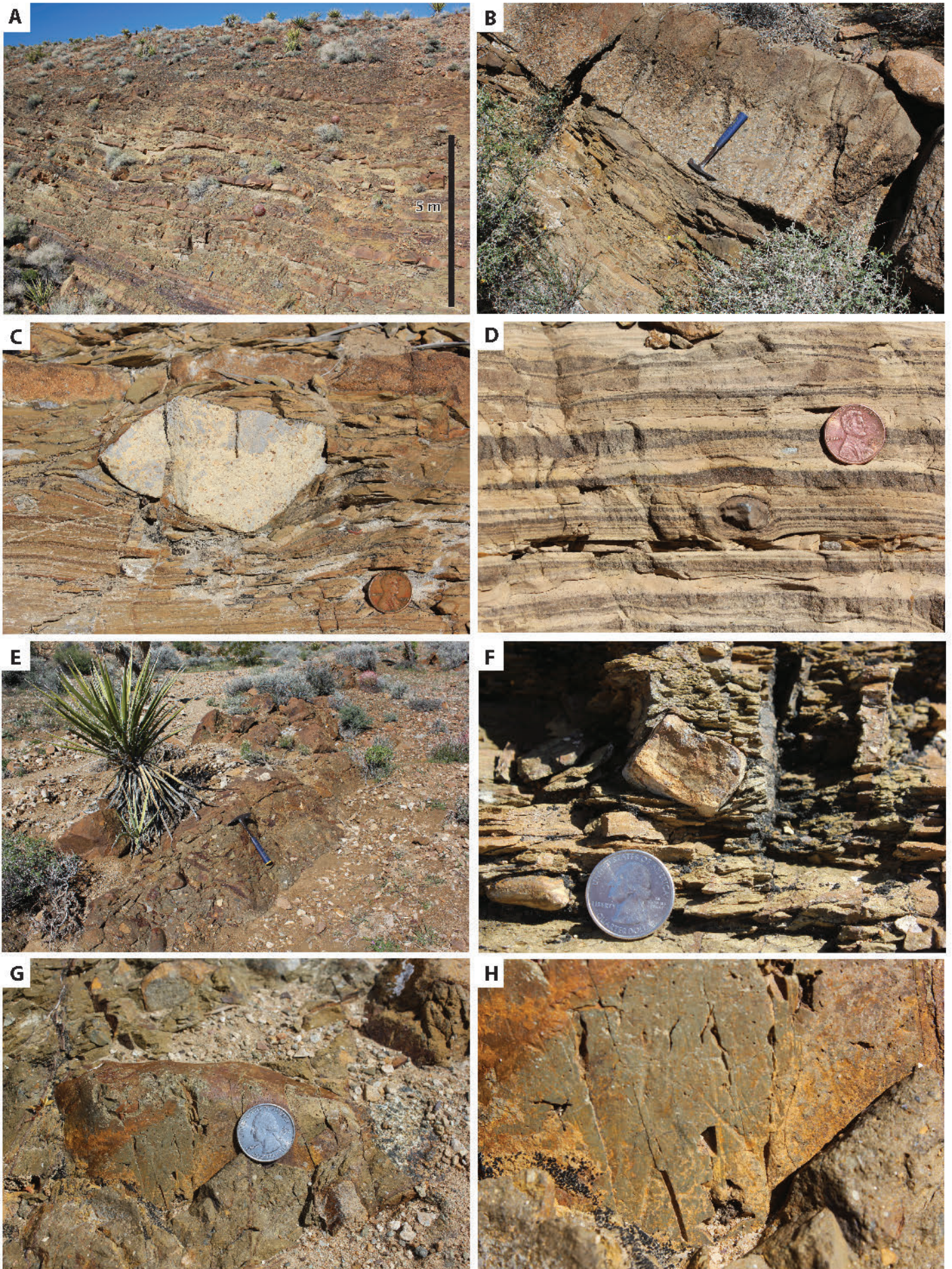
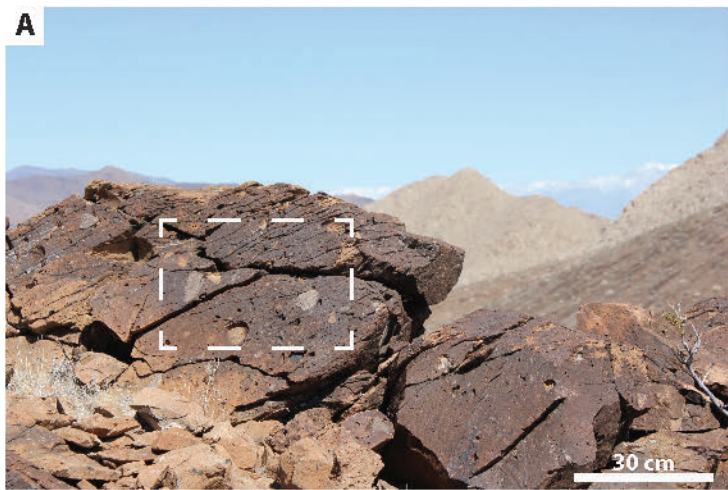
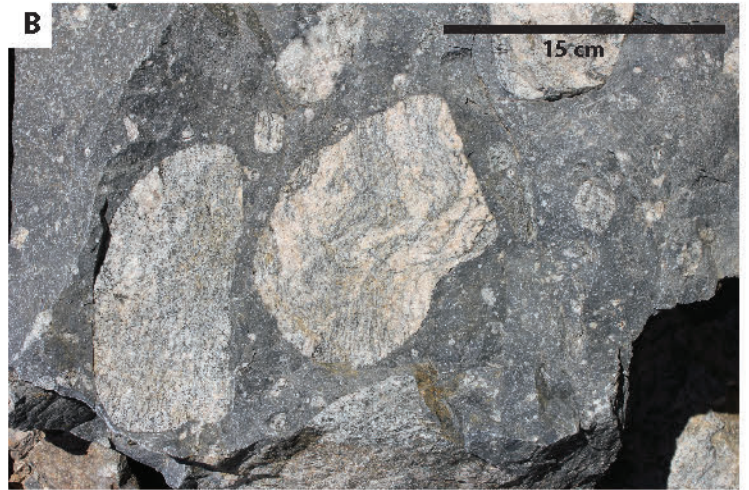


Figure 5





**Figure 6**



**Figure 7**

**Salt Spring  
Hills**

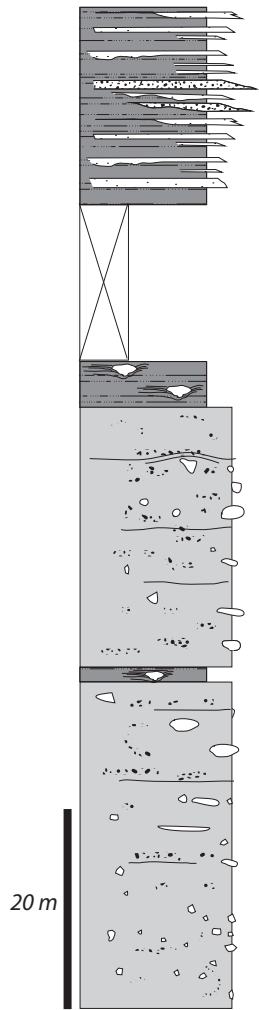


**Figure 8**





**Figure 9**



